ISSN 0281-2762

Transient spectral hole burning in Pr^{3+}:Y_2SiO_5

Master Thesis

by

Marito Olsson-Forsberg

Lund Reports on Atomic Physics, LRAP-354
Lund, January 2003

Abstract

This work presents the methods and results of an attempt to measure the oscillator strengths in $Pr^{3+} : Y_2SiO_5$.

$Pr^{3+} : Y_2SiO_5$ is a promising material in current efforts to create a quantum computer. The property which is to be exploited in the quantum computing scheme proposed by the group within which this work was done, is spin-polarization. To be able to create a polarization of the nuclear spins of the Pr^{3+}-ions, information about the oscillator strengths of the candidate material is crucial. This is the main object of the work in this report.

Contents

Chapter 1

Introduction

In the development of the quantum computer, one of the paths of exploration uses inorganic crystals doped with rare earth ions. The key to a scalable system for quantum computing in these materials lies in finding ways to isolate and control different populations of such ions through the use of frequency selective stimulation. Light of a certain frequency may be used to communicate with an ensemble of ions. Other ensembles may respond to other frequencies. These ionic ensembles are the carriers of the information to be treated by the quantum computer; they are the "qubits".

The mechanism exploited by the quantum computer to perform computations, is the "superposition of states"; the property of a quantum system to be "in two states at the same time". When two ensembles that are both in a superposition of states, are made to interact in a way that creates a correlation between them, the resulting quantum system is said to be "entangled". Entanglement is at the base of quantum computation, it is the very phenomenon that one wishes to exploit.

There are many different ways in which an atom can be in a superposition, for example: a superposition of electronic, vibronic or momentum states. In the case of the quantum computer, one needs to find a quantum variable in which it is possible to create a superposition and that is also readily detectable from the outside, for example through interaction with light.

In this search for a suitable parameter in the rare earth ion doped crystals (REDIC's), a superposition of spin states is the most convenient. In order to achieve this, a technique for controlling and changing the collective spin state of a specific population is needed. An ensemble that has all (or most) of the spin vectors of the individual ions pointing in the same direction is said to be spin-polarized. Spin-polarization is readily created in atomic gases and so is superposition and entanglement [3]. It is however not known how spin-polarization is best obtained REDIC's and to what extent it is controllable.

The starting point of this work was to investigate spin-polarization in the REDIC's. A prerequisite for designing schemes for the creation and control of the spin state of an ensemble is knowing the transition probabilities, or relative oscillator strengths for transitions between the hyperfine structure levels of an excited state and the ones in the ground state.

Many of these materials are presently under investigation for their promising quantum-optical properties. The photon-echo group in Lund has found Pr :

$Y_2SiO_5$to be particularly interesting. A calculation of the overlap integral for the $^3H_4 \rightarrow {}^1D_2$ in $Pr : Y_2SiO_5$ from a holeburning experiment performed by Longdell et al. [6], stated the $5/2 \rightarrow 3/2$ transition probability to be extremely small. The observations of the photon-echo group in Lund, however, contradicts this. For the design and execution of future experiments in this very promising substance, it is of central interest to get reliable knowledge of the magnitude of these oscillator strengths.

Theoretical data was collected and an experiment was designed to perform the necessary measurements in the chosen material. This report contains the results and conclusions from the experiments.

Chapter 2

Quantum computers

2.1 Introduction

The traditional computer technology, is based on microscopic transistors etched onto silicon wafers. It has been an ongoing technological revolution and success for the last fifty years or so. The amount of information processed per time and the number of electronic components per cm^2 has increased conjointly, following Moore's law. Gordon E. Moore, cofounder of the Intel corporation (together with Robert Noyce, coinventer of the integrated circuit), when asked by a magazine in 1965 about the future of electronics, predicted an exponential growth rate: The number of transistors per silicon chip doubles each year. In 1975, as the rate of growth began to slow, Moore revised his time frame to two years. His revised law was a bit pessimistic; over roughly 40 years from 1961, the number of transistors doubled approximately every 18 months.

However, we are now approaching the physical limits of this law. The dimension of the components on a chip (also known as the linewidth) is now less than 100nm. One has to use extreme ultra-violet light to be able to project these designs onto the silicon wafer. Reducing line-width also increases electric resistance, so cooling of the chip becomes a problem.

Current research in information technology is following two main tracks in the attempts to create ever more powerful computers:

One that builds on the silicon technology, but utilises it in a novel way, is the research on quantum dots and one-electron transistor. This path could permit continued augmentation of the packing density for still some time, however not indefinetily. One-electron devices still scafolds sequential computing. To make the real break-through in information technology, we would have to rethink computing altogether. This is what the other line of research does: the quest for a quantum computer.

Quantum computers where first suggested in the early 1980's by Benioff and Feynman. They showed theoretically that operations on quantum mechanical states could be used for calculation. Quantum mechanics is a powerful theory, but requires enourmous amounts of numerical calculations to make predictions or simulations of the outcome of an experiment. In order to overcome the numerical intractability of some problems, Feynman's original idea was to use a prepared quantum system to make calculations about the outcome of another

quantum system. This was the "point de départ" for quantum computing, a new way of thinking about calculation.

So, in what way would a quantum computer differ from the traditional computer? To see this we have to examine how the ordinary, binary computer works.

Principal characteristics of the traditional computer:

1. **Discrete, binary elements of information (bits).**

   A *bit* is the smallest element of information. It can have the binary value of either "1" or "0" , which physically is represented as "voltage" or "no voltage" over the transistor, for example.

2. **Sequential calculation.**

   By sequential calculation is meant that a computer can, in principle, only execute one arithmetical operation at a time. For example, it can be the addition of one number in a register with some other number in an other register. In some computer configurations, in supercomputers for example, one has enabled several calculation steps to be performed at the same time. This is done by having several processors work in parallel in a synchronized manner. Still only the same number of steps as there are processors can be performed in one time step.

Principal characteristics of the quantum computer:

1. **Information stored as a superposition of quantum states (the qubit).**

   The physical entity which is to carry the information is a specially selected and prepared quantum system - a *qubit*: an atom, an ensemble of atoms or ions or a photon with two distinct states. The two states can be used to represent for example the values *0* or *1*. Here the analogy with the traditional computer ends, for the peculiarity of the qubit is a quantum mechanical property called *superposition*. We are able to set the qubit in a state where it is "both" in the upper and lower state, simultaneously! Thus the qubit is both *0* and *1*. (See section 2.2.1)

2. **Quantum parallelism equals massive simultaneous calculation.**

   By putting several qubits in a superpositioned state, any operation carried out on them equals executing the same calculation with all the numbers that the qubit can represent. For example, a register of three qubits can represent all the numbers between 000=0 and 111=7, simultaneously. With two such registers and an operator, for example "addition", we could perform all possible sums of the numbers between 0 and 7; that is, for any number $n = 2^j$ that can be represented we can perform

$$\sum_{0}^{n} n;\ n = 0 \ldots (2^j - 1)$$

operations, in our case 36 sums, in one step. If the operator is non-commutational the number of operations becomes n^2 (n^k for k qubits); in our case 64 simultaneous operations.

2.2 Elements of Quantum Mechanics (QM) for quantum computers

2.2.1 Superposition of quantum states

A quantum-mechanical system, such as an atom or a photon, has a unique property which is never encountered in the macroscopic world: superposition of states. This could trivially be expressed as "the system is in two states simultaneously". For comparison, in the macroscopic world this would be like having a lightbulb with two definite states; either lit or unlit, and a third state which is an admixture of the previous: both lit and unlit. This is the property that researchers wish to exploit in order to create a quantum computer. A system in a superposition of states is the base for the minimal information carrier in the quantum computer - the qubit.

If an atom, for example, is to be used as a qubit, two energetic states have to be selected in such a way as to be conveniently accessible, e.g. it can be transferred between the states by a pulse of light. The information which is to be processed is then stored in the atom by giving it a pulse of light whos intensity is such that it would excite the atom in fifty percent of the cases, if performed repeatedly.

The classical example of superposition is the double-slit experiment, where a fringe pattern of interference lines is created by the particles that have passed the slits. Confirming the prediction of quantum mechanics (QM), the interference pattern arises equally well with particles, e.g. electrons, neutrons, atoms or molecules [2] as with more "wave-like" particles as the photons. The interesting part is that the pattern remains even if one sends the particles through the device one by one. It is as if the particle interferes with itself. It is impossible that the particle randomly goes through slit A or slit B, with a 50 % probability, since it would then "see" only a single slit and no pattern would be produced.

A position adopted by some is to say that the particle goes through both slits at the same time, although this is an oxymoron; a particle should be a localized entity. There is no operational meaning in such a statement. One way of looking at this would be to say that it is the probability wave of the only particle which goes through both the slits.This would be in accordance with the non-locality principle of QM. However, what the concept of such a "probability wave" really means is difficult to penetrate for the rational mind. It leads to questions about the essence of *being* and *knowing* and connects the natural sciences with the philosophical fields of ontology and epistemology in an intricate manner. This, and a lot of other unconfortable consequences of QM has been, and still is, matter of profound philosophical discussions. [2, 17]

An other interesting example of the consequences of superposition is the experiment depicted in figures 2.1-2.3 [20]. In an attempt to determine which way a single photon travels, we begin by setting up a beam-splitter and two detectors. 50% of the light goes to detector 1 and 50% to the other one and photons are registered with equal probability in either detector.

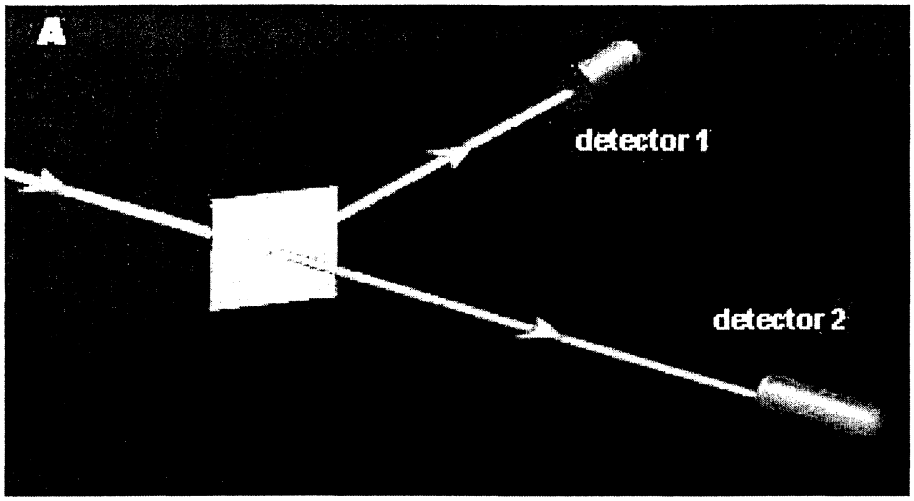

Figure 2.1: Single photon reflected off a 50-50 beamsplitter.

What can we say about the single photon? In this case it seems resonable to assume that in half of the cases it goes to detector 1 and in the other half to detector 2. By adding two mirrors and an other beam-splitter, we can however show that the photon, or at least something related to the photon (probability or information perhaps?) goes "both ways" (see figures 2.2, 2.3).

By focusing the two beams at the surface of the second beam-splitter and placing the detectors in line with the two beams an other sort of quantum interference phenomenon can be observed. If the previous assumption that a photon goes to detectors 1 and 2 with an equal probability of 50%, then we should still see the same distribution with the new setup. That is not what happens. If the two paths are exactly equal in lenght, then it turns out that there is a 100% probability that the photon reaches detector 1 and 0% that it reaches detector 2! The photon is certain to strike detector 1! It seems inescapable that the photon must, in some sense, have travelled both routes at once, for if an absorbing screen is placed in the way of either of the two routes, then it becomes equally probable that detector 1 or 2 is reached.

Blocking one of the beams allows detector two to be reached; with both routes open the photon somehow "knows" it is not permitted to reach detector 2, so it must have actually felt out both routes. It is therefore perfectly legitimate to say that between the two beam-splitters, the photon takes both paths. In a quantum mechanical language this is equivalent to the statement that the photon is in a coherent superposition of being in the transmitted beam and in the reflected beam.

In the same way an atom can be prepared to be in a superposition of two different electronic states, and in general any two-level quantum system used as a quantum information bit, called a qubit, can be prepared to be in a superposition of its two logical states 0 and 1. Thus one qubit can encode at a given moment both 0 and 1.

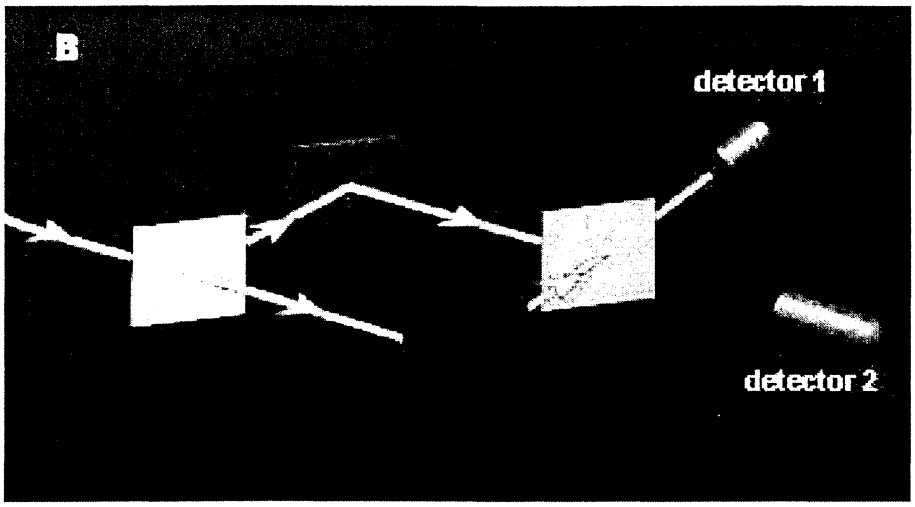

Figure 2.2: Photon strikes with certainty detector 1.

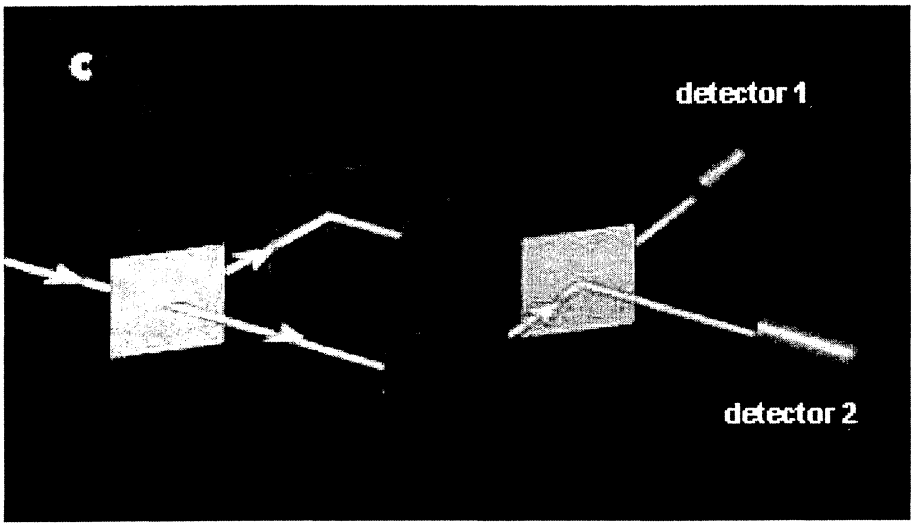

Figure 2.3: If one path is blocked, the photon strikes detector 1 and detector 2 with equal probability.

2.2.2 The Hadamard transform

The beam-splitter experiment mentioned in the above is the base for some of the one-qubit transformations that underpin the construction of logical gates for qubits: one of these transformations is the Hadamard transform.

$$H|0> \rightarrow \frac{1}{\sqrt{2}}(|0> + |1>). \quad H|1> \rightarrow \frac{1}{\sqrt{2}}(|0> - |1>) \tag{2.1}$$

The above equation describes the action of the beam-splitter. This means that if we know the particle/qubit to be in a
superposition, $|Q' >= \frac{1}{\sqrt{2}}(|0 > +|1 >)$, we can chose a new basis of eigenfunctions that is rotated by $\frac{\pi}{4}$ in Hilbert space with respect to the first basis, and in this basis the qubit is in a welldefined state. This would be the inverse of the Hadamard transformation above.

2.2.3 Non-locality

The examples in sections 2.2.1 and 2.2.2 clearly show that unavoidably, some entity with properties not dependent on the location of the particle is at action in such quantum mechanical systems which display the symptoms of superposition of states. This is usually called the non-locality aspect of quantum information.

This property leads to situations where our conventional, macroscopic sense of causality and locality are stretched, if not violated.

2.2.4 Entanglement, non-locality and the hidden variable theory

The concept of entanglement and the problem of non-locality became intrinsic parts of quantum mechanic theory very early in its history.

It was realised from the first formulations of QM by Erwin Schrödinger and Werner Heisenberg in 1926 that novel, counterintuitive phenomena was predicted if one applied this theory to the letter. Einstein, who wasn't ever very fond of QM argued first, in his famous dialogue with Bohr, that QM is inconsistent, i.e. that the application of its postulates eventually leads to apparent contradictions. He later opted to consider it an incomplete theory. Almost ten years had gone by, when Albert Einstein, Boris Podolsky and Nathan Rosen (EPR), in an article published in The Physical Review, demonstrated that some of the postulates of QM lead to physical situations such, that this theory must be an incomplete description of reality [1]. This means that they attacked the so called "completeness postulate" of QM, which states that the wavefunction of the system contains all the (measurable) information about the system.

In their paper, EPR consider systems consisting of two particles such that, while neither their individual positions nor momenta are well defined, the sum of their positions, that is their centre of mass, and the difference of their momenta, that is their individual momenta in the center of mass system, are both precisely defined. This is the formal definition of a QM system in a state of entanglement[1]. Mathematically this would be expressed:

$$\begin{aligned} < (X_1 + X_2) > &= X \\ < (P_1 - P_2) > &= P \end{aligned}$$

where X and P are constant.

This could for example be the case of a particle with a defined (measured) position decays into two particles travelling in different directions. In some frame of reference (the lab system) the initial particle was at rest. We thus know that

[1]The word entanglement comes from the german "Verschränkung", a term introduced in 1935 by Schrödinger to characterise this special feature of composite quantum systems.

this position is the center of mass for the new system, after the decay, and also that the sum of the momenta of the new particles is zero.

$$\begin{aligned} < (X_1 + X_2) > &= X(t = 0) \\ < (P_1 - P_2) > &= 0 \end{aligned}$$

If we now perform a measurement of the position of particle 1 in this couple, we also get information about the position of particle 2, without measuring it. In fact, our measurement "causes" the second particle to be in an exact location. The same thing is true if we measure the momentum of one of the particles. Assuming that the two particles can be separated by arbitrary distances, EPR suggest that a measurement on particle 1 cannot have any actual influence on particle 2. This is the *locality condition*. Thus the property of particle 2 must be independent of the measurement performed on particle 1, EPR then argued. This is also what seems intuitively right. To EPR it then follows that both position and momentum can simultaneously be well defined properties of a quantum system. This implies that either QM is inconsistent, i.e. leads to contradictions with its own postulate (which in this case would be a violation of the Heisenberg uncertainty principle) or it is incomplete, i.e. some unknown variable exists which is not accounted for in present-day QM theory (and that we have not yet been able to measure), which permits simultaneous definition of both momentum and position.

The respons of Niels Bohr was that, since the two particles in the EPR case are always parts of one single quantum system, measurement on one particle changes the possible predictions that can be made for the whole system and therefore for the other particle. (For a system to remain in an entangled state, it necessarily has to be prevented to interact with other particles. This is a condition which constitutes one of the obstacle for the construction of quantum computers.)

Einstein was reluctant to accept quantum mechanics. *Gott würfelt nicht* - God doesn't play dice; in his opinion the probabilistic view of the world that QM imposed was unæsthetic or at least counterintuitive.

With the EPR article, Einstein started to turn his critics of QM away from the inconsistency path and towards an incompleteness argument. The idea of a hidden, local, variable is almost explicit in the EPR article. Eventually his quest for a hidden variable theory to explain the predicted correlation between spatially separate systems, would become manifest. He was very fond of this explanation, which permitted a unification of the QM picture with classical physical thinking.

The thought behind the hidden variable theory is that the state of every system is in some way determined even before measurement. The actual values of position (the path) and momentum of the two particles would then already be fixed at the moment of creation, when the initial particle decays. The value of these variables for each particle would be determined by a new, unmeasurable, variable (thus the *hidden* variable), with only local influence in the vicinity of the original "mother"-particle.

What happens at the measurement of a variable is what is usually called the collaps of the wavefunction. Let's for a moment consider a single, non-entangled system. Before measuring it, the particle is in a superposition of its possible states (for example $|0\rangle$ and $|1\rangle$). It is not until it interacts with the detection

device that its wavefunction collapses to one of its eigenstates.

$$\Psi = \frac{1}{\sqrt{2}}(|0> + |1>) \rightarrow \Psi = |0> \text{ or } \Psi = |1> \tag{2.2}$$

The difference in the EPR example is that the wavefunction doesn't have the appearance of equation 2.2. It consist of terms that involve parts of the possible states of both particles, a so called *product state.* For simplicity, we switch to a two-level example instead of the continuous variables (x and p) of the original EPR *gedanken* experiment. The result of the demonstration is much the same but clearer to the eye. The wavefunction of an entangled pair would then be:

$$\Psi = \frac{1}{\sqrt{2}}(|0>_1 |1>_2 + |1>_1 |0>_2) \tag{2.3}$$

The particularity of the product state described by equation 2.3, which models entanglement, is that it cannot be produced by the mere multiplication of wavefunctions of two separate systems and, hence, cannot be factorized either. That is, there is no algebraic operation built into the theory which can separate the wavefunctions, and thus the information, of the two particles.

2.3 QC scheme in rare-earth-doped inorganic cryl-stals

A proposal for implementing larger structures of interacting qubits is proposed by Ohlsson, Mohan and Kröll [19]. This scheme is based on selecting populations of rare-earth ions with specific frequency properties, using laser pulse sequences. Each population acts as one qubit and is homogeneous with respect to a specific resonance frequency, and also in relation to the frequency shifts induced in other populations through dipole-dipole interaction. By means of these frequency shifts different qubits can interact, making the realisation of quantum C-NOT gates possible.

Elements of the lanthanide group have what is called 4f contraction [7]. (See figure 3.2) For these elements we have complete 5s(5p) shell(s), while the lower lying 4f shell is still not filled. Electrons in the 4f shell are thus electrically shielded by the 5s and 5p shells, as if in a Faraday cage. This accounts for the very sharp homogeneous spectral linewidths for transitions within the 4f shell, even when the lanthanide ion is doped into a crystal. For a further look at this phenomenon, see section 3.3

In crystals, due to lattice defects and unevenly distributed, possibly clustered ions, the absorption frequency of the rare-earth ions is inhomogeneously broadened. The combination of very sharp homogeneous linewidth with very large inhomogeneous broadening of the line makes rare earth doped crystals a suitable material for quantum computing.

Indeed, every resolvable homogeneous line under the inhomogeneous linewidth can act as one channel, one qubit. This channel thus consists of a population of ions, with random spatial distribution but with correlated response to radiation of certain frequencies. An inhomogeneous linewidth of the order of GHz and a homogeneous linewidth in the order of kHz, which is the case for most lanthanide ions, gives a theoretical possibility of millions of channels in a single crystal.

Each population is thus selected by adressing a sharp absorption frequency under the inhomogeneous bandwidth.

The excitation of one population causes a change in these ions' permanent electric dipole moment. The local field is altered and this in turn induces a frequency shift (Stark shift) in surrounding ions, even in those of other resonance frequencies, thus giving us a mechanism for qubit interaction. By carefully selecting populations with correlated frequency shifts, a scalable scheme for quantum computation is proposed.

2.3.1 Population selection

The two-level system chosen for the qubit would be hyperfine-levels in the ground state of a rare-earth ion. These levels can be arbitrarily labelled $|0>$ and $|1>$. For the operations of the scheme proposed by, [19] a third, auxiliary level is needed in the ground state, $|aux>$. Therefore we need to use only rare earth ions with $I \geq 2$, for example Pr^{3+} or Eu^{3+}.

In the chosen excited state, which in Pr^{3+} would be $^1D_2$, we need only use one level for the optical transition and, depending on population selection, this can be either of the three hyperfine levels.

The separation between the ground state hfs-levels in Pr^{3+} is 17.3 MHz and 10.2 MHz respectively. As $kT(T = 4K) \approx 100GHz$, the ground state levels can be considered equally populated at the temperatures where these experiments are conducted. Before creating interacting qubits, a pure quantum state is needed. By irradiating the crystal with two optical fields with a frequency difference of $10.2MHz$, optical pumping of the population to the third hyperfine level $|0\rangle$ is created. (See figure 2.4a). Due to the extremely long lifetimes in the ground state hfs-levels ($\sim$ minutes to hours), there is ample time for qubit operations to take place.

2.3.2 Qubit interaction

Qubits consisting of hyperfine levels in different populations do not interact, except if prepared to do so. That is; the passage $|0\rangle \rightarrow |1\rangle$ will not induce a shift in the absorption frequency of the other qubit, but the transfer of the first qubit to the $|exc\rangle$state, through an optical π-pulse will.

This preparation is described in figure 2.4b. First, two channels, C and T, with slightly different optical transition frequencies have been arbitrarily selected. Optical pumping selects ions responding to these frequencies and places them in the $|0\rangle$-state.

Next, ions from these two populations that are at proper distance to induce a correlated frequency shift through dipole-dipole interaction are selected by the following procedure (see figure 2.4b):

1. Ions in channel C are put in the upper,$|exc\rangle$-state by means of a $\pi-$pulse. Ions in channel T situated close enough to C-ions will have their absorption frequency shifted by a certain amount, and will no longer absorb at their original frequency. T-ions with no neighbouring C-ions will however still absorb.

2 and 3. The T-ions that have not been shifted are rejected from the qubit and put in the $|exc\rangle-$state through optical pumping.

4. C-ions are returned to the ground state through an other $\pi-$pulse. This makes the T-ions that were originally shifted out of their resonance frequency by

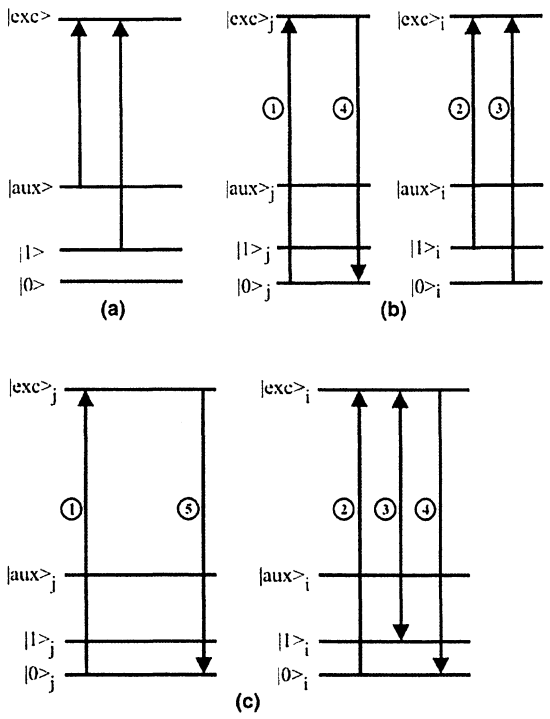

Figure 2.4: Qubit preparation scheme in a rare earth ion doped crystal: a) Optical pumping, b) Population selection, c) Pulse sequence for a C-NOT gate.

pulse nr.1 return to their normal frequency. After this procedure, the frequency of the C-ions clearly can be used to control the state of the T-ions. If this procedure is now repeated in the reverse manner, the remainder of the T-ions will then control the C-ions and we get a pair of channels/qubits that control eachother mutually.

Theoretically the creation of a large number of such qubit-pairs is possible through the repetition of this sequence at different frequencies.

2.3.3 Pulse sequence for a controlled-NOT gate

This pair of codependent qubits can be used to implement the Controlled-NOT gate (C-NOT). To perform a C-NOT operation with the C-ions as control bit and the T-ions as target bit, the manipulations of the qubit pair constructed above would be (see figure 2.4c):

1. $\pi-$pulse to do $|0>_C \rightarrow |exc>_C$
2. $\pi-$pulse to do $|0>_T \rightarrow |exc>_T$
3. $\pi-$pulse to do $|1>_T \rightarrow |exc>_T$
4. $\pi-$pulse to do $|exc>_T \rightarrow |0>_T$

5. $\pi-$pulse to do $|exc>_C \rightarrow |0>_C$

Chapter 3

Theory of hyperfine levels

3.1 Introduction

3.1.1 Energy levels of the free ion

In a free atom or ion which has a resultant electronic angular momentum J, and a nuclear spin I, the two are generally coupled together through the magnetic interaction between the electronic and nuclear dipole moments. Within a manifold of a given J this usually takes the form

$$H = a(\mathbf{J} \cdot \mathbf{I}) \tag{3.1}$$

which couples **J**,**I** together to form a set of levels with quantum numbers $F = (J+I), (J+I-1), ..., |J-I|$. The energy of a level with quantum number F is

$$E_F = \frac{1}{2}\left(F(F+1) - J(J+1) - I(I+1)\right) \tag{3.2}$$

and this gives a separation between levels of

$$E_F - E_{F-1} = aF \tag{3.3}$$

which is similar to the Landé interval rule for the fine structure splitting. If $J, I \geq 1$, the electronic system and nucleus may possess electric quadrupole moments, and their interaction gives a coupling different from equation 3.1. The splitting of the hyperfine multiplet then no longer obeys the interval rule (3.3).

3.1.2 Zeemansplitting of hyperfine levels

A weak external magnetic field **B**, sufficiently small that the Zeeman energy is small compared to the hyperfine energy, splits each manifold of $2F+1$ states belonging to a given F value by an amount proportional to **B**. The manifold behaves as if it had a magnetic dipole moment

$$\mu_F = -g_F \beta \mathbf{B} \tag{3.4}$$

where g_F is a Landé factor which takes into account the coupling between the nuclear and electronic magnetic moments through their respective Landé factors,

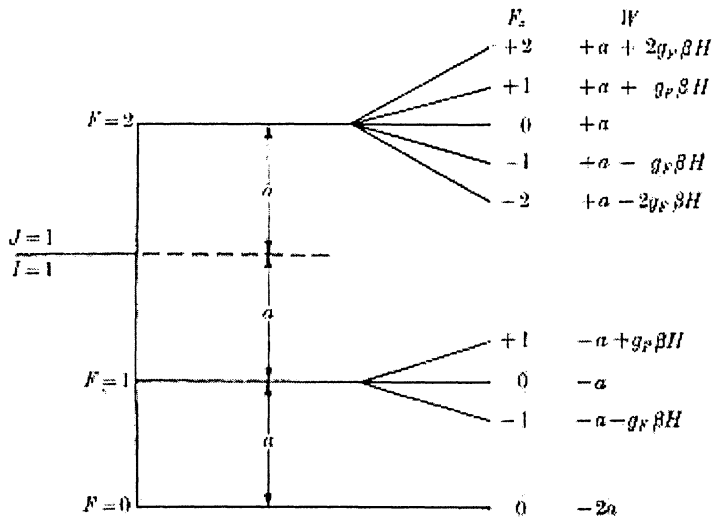

Figure 3.1: Magnetic hfs multiplet for the system $J = 1$, $I = 1$ corresponding to the hamiltonian (3.1), with weak field zeeman splitting. [7]

g_I and g_J.

$$g_F = \frac{F(F+1)(g_J - g_I) + (J(J+1) - I(I+1))(g_J + g_I)}{2F(F+1)} \tag{3.5}$$

Since g_I is about 1/1836 of g_J, equation 3.5 can often be simplified as

$$g_F = g_J \frac{F(F+1) + J(J+1) - I(I+1)}{2F(F+1)} \tag{3.6}$$

The energy difference of adjacent hyperfine levels is of the order $10^{-3} - 10^{-1}\ cm^{-1}$. Experiments on crystals are in most cases carried out at 4K (liquid helium temperatures) where $kT \approx 3\ cm^{-1}$. Hence in all following cases, we can consider all the levels of a hyperfine multiplet to be equally populated.

3.2 Hyperfine levels in crystals

Due to the crystal field, which is an electric field generated by the atoms forming the lattice, the angular momentum, J, of the electrons in the shell is "quenched". This means that the magnetic dipole moment M_J which exists in atomic conditions is no longer a good quantum number. Since the coupling between the crystal field and J; and between the crystal field and the nuclear spin, I, respectively, is much stronger than the magnetic coupling between J and I, this latter interaction is smothered. We cannot speak of a total angular momentum, $F = J + I$, nor of a resulting magnetic quantum number, M_F, under these conditions. [7]

The hyperfine structure of an ion in a crystal will thus be determined solely by its nuclear angular (spin) momentum, I, which couples directly with the

crystal field. In the case of Pr^{3+}, the nuclear spin is $I = 5/2$. All electronic levels will have a sixfold degeneracy [1] which is alleviated by the crystal field. The crystal field at the site of the Pr^{3+} ion produces a Stark effect which separates states with different $|M_I|$ values for each electronic level. The result is a hyperfine structure of three doubly degenerate levels; $M_I = \pm\ 1/2, \pm\ 3/2, \pm\ 5/2$. This degeneracy may in turn be lifted if an external magnetic field is applied (Zeeman effect).

3.3 Rare Earth ions in Crystals

3.3.1 The Rare Earths

Introduction

The rare earth elements (RE) are a series of elements from group 3B in the periodic system. They are chemically similar, Barium-like [21] and have in common an open 4f shell. They are mostly trivalent and it is principally the properties of the trivalent ion which are important, rather than those of neutral atoms. All trivalent RE-ions have in common the xenon-like rare gas structure of 54 electrons in completely filled shells and contain, in addition, N 4f electrons, with N ranging from zero (La^{3+}) to fourteen (Lu^{3+}). The group is also known under the denomination "lanthanides", from the name of the first atom of the group, Lanthan, which together with the last, Lutetium, is considered by many as not strictly belonging to the rare earth group.

The thirteen RE in the strict sense (Ce to Yb), which have, thus, a partly filled 4f shell, all have very similar though not identical chemical behavior, so that it was previously considered very difficult to separate them. Questionnable purity of RE sample used in spectroscopy was an issue for the first fifty years or so of research.

3.3.2 Spectra of Rare Earth ions in crystals

[2]Pure line spectra are best observed in dilute gases. Here atoms are so far from each other that their properties are those of the isolated atom. The linewidth is the natural width modified by the Dopplershift. The natural line width is due to the finite lifetime of the excited state.

$$\delta\nu_N = \frac{1}{2\pi\tau}$$

When gas pressure is increased, lines begin to broaden under the effect of pressure or collision broadening. The higher probability for collision and subsequent desexcitation shortens the average time spent by the atom in the upper state, thereby increasing the uncertainty in energy of this level.

When pressure rises further, lines will broaden to such an extent as to begin overlapping neighboring lines and we obtain a continuous spectrum with no noticeable structure. This is usually true for liquid and solid state substances;

[1]We get $M_I = \{I, I-1, ..., -I\}$, that is $(2I+1)$ states.

[2]Unless otherwise indicated, the material of the following theoretical overview (sections 3.3.2 - 3.3.6) has been collected in [7], [15], [22] and [23].

liquid metal has a continuous emission spectrum and a NaCl crystal has a continuous absorption spectrum.

Reasons for broadening in solids have several, often interdependent, causes. Close proximity between ions produces large Stark shifts of the levels of the individual ion. This however would still produce sharp lines if the field was constant. However, the more or less arbitrary distances, combined with thermal motion of the ions average the positions of the lines, causing a continuous spectrum. This could lead to the conclusion that sharp lines would be produced if only the crystal was cold enough. In most cases this in not true due to resonance interaction. This means that neighboring atoms can interact since valence electrons in the crystal are not strictly localized in the vicinity of one nucleus, but is partly shared by the neighbors. In metals, this goes so far as to have electrons completely free to move inside the crystal.

Considering the above, it is not difficult to see under what conditions such sharp lines are expected.

Firstly, the atom or ion in question must have a regular surrounding which is not subject to fluctuations in time and is the same for all atoms of the same kind. This condition is fulfilled for crystals at very low temperatures. Since the subject of this report refers to spectra from ions, I will from here on mostly use this word, thereby not implying that what is said couldn't be valid also for neutral atoms and molecules.

Secondly, and more importantly, neighboring ions of the same kind should not interact markedly. This means that the "valence" electrons, that is, the electrons responsible for the emission and absorption, are screened from those of their neighbors. In the quantum mechanic language this means that the wavefunctions of these electrons of neighboring ions must not appreciably overlap. In a classical picture, it means that these electrons must be in inner orbits protected by outer electrons. (See figure 3.2.)

Thus there are some solid substances that display sharp spectral lines, of which the rare earth ion doped inorganic crystals (REDIC) form an important group. The 4f orbits lie well inside the electronic shell and are well protected. The approximation of an isolated ion perturbed only by the crystal electric field is therefore better for the lanthanide than in any other case.

There is, of course, a difference between the behavior of a free ion and that of the same ion forming a part of a crystal lattice. The ion in the crystal is coupled to the lattice, which means that part of its energy can be transferred to the lattcie in the form of lattice vibration or vibrations of molecular complexes.

For this reason, we shall try first to find cases where these interactions, though they are never absent, are reduced to very small amounts. In such cases we may regard the ion in first approximation as being a free ion in an electrostatic field produced by the neighboring crystal ions. We shall see that the symmetry of this electrostatic field is of great importance for the structure of the energy levels in the crystal.

In the REDIC the perturbation of the crystal field is generally to be considered small, compared to that of the spin-orbit interaction.

History

The extreme sharpness of the spectral lines in rare earth compounds (REC) have attracted physicists since the early days of spectroscopy. Among other

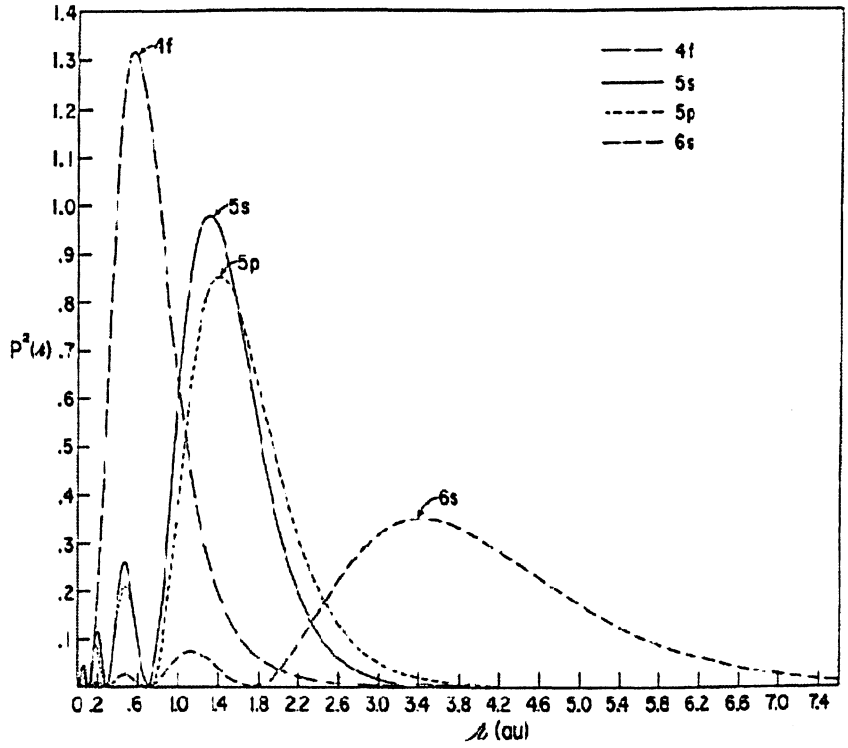

Figure 3.2: Contraction of the wavefunctions for the $4f$-electrons characteristic of the rare earths. This is the "screening"-effect that can produce sharp spectral lines for these electrons. [15]

investigators, J. Becquerel found in 1906 that the absorption lines of REC cooled down to liquid air temperatures (85 K) can be as narrow as those of free atoms or ions. A few years later he discovered that many of these crystal absorption lines show a considerable Zeeman splitting in a magnetic field.

The theoretical treatment of spectra progressed enormously with the advent of the Bohr model in 1913 and later with the introduction of quantum mechanics in 1926, but it was not until 1930, through the works of Bethe and Kramers, that a description of the observed phenomena in the REC became possible. It was Bethe who showed that the observed splitting of the absorption lines in the crystal field is connected with the symmetry of this field. It was also gradually understood that all the sharp-line features of the REC's came from forbidden transitions in the 4f shell.

After World War II, theoretical foundations were further clarified, primarily by K. H. Hellwege. Microwave absorption and paramagnetic resonance studies gave details about transitions between Zeeman levels of the ground state (Bleaney and others).

Later, even more sensitive spectroscopic techniques, such as photon echoes and hole burning spectroscopy, have further increased the experimental resolu-

tion.

The major theoretical task has been the problem of attributing the correct transition to each of the many observed lines. The modification of the states of the free ion by the crystal field is calculated through ordinary perturbation theory. The complexity of the different types of interactions in these ions leads to a need to consider often more than 3000 wavefunctions (for ions in the middle of the lanthanide group) in calculations of the energy levels. Systematic methods for simplifying these calculations have therefore been of great interest, and were developed mainly by Racah (1942-1949). The so called Racah-algebra introduced 3j, 6j and 9j symbols to simplify the handling of the crystal field hamiltonian. Group theoretical analysis was then used to exploit all possibilities of simplification that comes with symmetry aspects of the system. The calculation of energy levels was then possible with a sufficient accuracy in most cases for the identification of the empirical levels, at least the lower ones.

The determination of the wavefunctions is a much harder problem. There is no direct empirical method to determine the wavefunctions of the observed states. These always come from fitting theoretical expressions to a finite number of empirical data. At the present, the main theoretical venture is the adaption of empirical parameters to theoretically calculated wavefunctions, sometimes from several different models simultaneously [6]. These empirically corrected wavefunctions are then used to develop computer programs which may predict spectral behavior of REC's under different conditions (such as transition probabilities, selection and polarization rules and their behaviour under the influence of external fields) with increasing accuracy [24, 25]. These programs are in turn used to make predictions of how some of the extraordinary properties of different REC's may be optimized and to learn how they can be fruitfully employed in new applications [8, 9, 10].

The understanding of the spectra of the RE elements has experienced an accelerating growth during the last century. However, scientists in this area seem to concur that for most RE-atoms and ions, the major part is yet to be done!

3.3.3 The crystal field: electrostatic model

As mentioned above, to a first approximation, the ion is considered to be in a static electric field produced by the neighboring ions, the crystal field. Dynamic interactions with the lattice or with other ions or molecular complexes are not considered. This is the electrostatic model for the crystal field, which accounts for most of the observed features in the crystal spectra. The approximation implies:

1. We have a perfect crystal. (No broadening due to lattice tension from defects in the lattice)

2. No lattice vibration. (Working only close to 0 K temperature.)

The hamiltonian of the ion in the crystal is, as usual, constructed from the free ion hamiltonian with the addition of the hamiltonian of the crystal field potential treated as a small perturbation.

$$H = H_{FI} + H_{CF} \tag{3.7}$$

The free ion hamiltonian consist of three elements: $H_{FI} = H_{cf} + H_{coul} + H_{LS}$. H_{cf} is the central field approximation. Since it's the zeroth order approximation, the label H^0 is sometimes seen in the litterature. H_{coul} and H_{LS} represent the perturbations added by the electrostatic repulsion between outer electrons (coulomb repulsion) and the spin-orbit interaction. Since these are often labelled H^1 and H^2, the contribution from the crystal field is sometimes called H^3, without further explanation.

The theoretical development based on the electrostatic model of the crystal field has been made in several different ways, by different authors. In the litterature, one may encounter different symbols and parameters of which I will make a brief description here.

3.3.4 Group theory and symmetry.

A free ion level with total angular momentum J is $(2J + 1)$-fold degenerate. Part or all of this spatial degeneracy is removed by the crystal field, because this always has less than spherical symmetry. As the crystal field is an electric field, this is a result of the Stark effect. The number of components depends on the symmetry of the crystal field. In very general terms, one may say that, the lower the symmetry of the field, the more the degeneracy is lifted.

The symmetry of the crystal field is one of the 32 crystallographic point groups (see table 3.3). This may or may not have the same symmetry as the basic unit of the crystal structure. In our case, $Pr^{3+} : Y_2SiO_5$, we have C_{2h}symmetry for the base unit but only axial (C_1 or D_∞) symmetry of the field at these sites.

The application of group theoretical methods to the spectra of crystals is briefly as follows. A symmetry operation is a coordinate transformation which produces no physical change in the system. This rather vague definition is equivalent to saying that the symmetry operation S must commute with the hamiltonian H of the system. All the possible symmetry operations of an ion in a crystal field form a *group*, one of the crystallographic point groups or a group closely related to them.

An abstract group is defined only by the multiplication table of the group elements with no regard to the particular geometric or physical significance of the operation. *Representation theory*, however, deals with matrices which when multiplied with each other by ordinary matrix multiplication, obey the same rules as the elements of the abstract group. There are an infinite number of such representations by matrices for each abstract group. These matrices may be changed, by a coordinate transformation, into other matrices which perform the same operation. Such matrices are called equivalent matrices and they have identical group properties. All of these representation matrices can be brought to diagonal form by a unitary transformation. If a transformation can be found that brings all matrices into submatrices along the diagonal, we call the representation *reducible*, and a set of individual submatrices but of smaller dimension than the original representation will also form a representation of the group. When this simplification is not possible, the representation (the set of matrices) is *irreducible*.

The groups important for crystal symmetry are mostly related to the cyclic groups C_g, where the generating element a represents a rotation about a fixed axis through an angle $\frac{2\pi}{g}$ and the group consist of a and all its powers up to $a^g = e$. For crystal symmetry, only C_1, C_2, C_3, C_4 and C_6 occur.

			Number of elements of order							Irr. repr. dim.				
	S^b	HM^a	1	2	3	4	6	g	n_c	1	2	3	J^d	Isomorphism
Triclinic														
1	C_1	1	1	—	—	—	—	1	1	1	—	—		
2	C_i	$\bar{1}$						2					J	C_2
Monoclinic														
3	C_2	2	1	1	—	—	—	2	2	2				
4	C_s	m						2						C_2
5	C_{2h}	$2/m$						4					J	$D_2 = C_2 \times C_2$
Orthorhombic														
6	D_2	222	1	3	—	—	—	4	4	4	—	—		$C_2 \times C_2$
7	C_{2v}	$mm2$						4						$D_2 = C_2 \times C_2$
8	D_{2h}	$2/m\ 2/m\ 2/m$	1	7	—	—	—	8	8	8	—	—	J	$C_2 \times C_2 \times C_2$
Rhombohedral														
9	C_3	3	1		2	—	—	3	3	3	—	—		
10	C_{3i}	$\bar{3}$						6					J	$C_6 = C_3 \times C_2$
11	D_3	32	1	3	2	—	—	6	3	2	1	—		
12	C_{3v}	$3m$						6						D_3
13	D_{3d}	$32/m$						12					J	D_6
Tetragonal														
14	C_4	4	1	1	—	2	—	4	4	4	—	—		
15	S_4	$\bar{4}$						4						C_4
16	C_{4h}	$4/m$	1	3	—	4		8	8	8		—	J	$C_4 \times C_2$
17	D_4	422	1	5	—	2	—	8	5	4	1	—		
18	C_{4v}	$4mm$						8						D_4
19	D_{2d}	$\bar{4}2m$						8						$S_{4v} = D_4$
20	D_{4h}	$4/m\ 2/m\ 2/m$	1	7	—	8	—	16	10	8	2	—	J	$D_4 \times C_2$
Hexagonal														
21	C_6	6	1	1	2	—	2	6	6	6	—	—		
22	C_{3h}	$\bar{6} = 3/m$						6						S_6, C_6
23	C_{6h}	$6/m$						12	12	12	—	—	J	$C_6 \times C_2$
24	D_6	622	1	7	2	—	2	12	6	4	2	—		
25	C_{6v}	$6mm$						12						D_6
26	D_{3h}	$6m2$						12						D_6
27	D_{6h}	$6/m\ 2/m\ 2/m$	1	15	2	—	6	24	12	8	4	—	J	$D_6 \times C_2$
Cubic														
28	T	23	1	3	8	—	—	12	4	3	—	1		A_4
29	T_d	$\bar{4}\,3m$						24						O
30	T_h	$2/m\,3$	1	7	8	—	8	24	8	6	—	2	J	$T \times C_2$
31	O	432	1	9	8	6	—	25	5	2	1	2		π_4
32	O_h	$4/m\,\bar{3}\,2/m$	1	19	8	12	8	48	10	4	2	4	J	$O \times C_2$

[a] 18 different groups.
[b] S = Schoenflies symbol.
[c] HM = Hermann-Maugin (International) symbols.
[d] (J) This column indicates presence of center of symmetry.

Figure 3.3: The 32 crystallographic point groups. Source: [15]

All the non-cubic crystallographic groups are simple extensions of the cyclic group, which are obtained by adding to the elements, a, of the cyclic group one or more generating elements b, c of order 2. The geometrical signification of these elements is a rotation about a twofold axis, a reflection in a symmetry plane, or an inversion in a point. They always obey the rule $b^2 = e$

Each of the irreducible representations of a group is usually labeled Γ_n, n being the number of a particular representation. The fundamental connection between group theory and quantum mechanics is that for a particular symmetry represented by a symmetry group, each energy level belongs to a particular irreducible representation. This is why in many theoretical articles, levels are labeled Γ_1, Γ_2 etc. , thereby connecting the level to its corresponding irreducible representation. This is most common when one of the cubic groups is used.

An important symmetry aspect is the Kramers degeneracy also called time

reversal symmetry. Kramers' theorem states that:

If the ion has an odd number of equivalent electrons (electrons with the same n and l quantum numbers), all states (in one J-manifold) are degenerate because of time reversal symmetry.

This has to do with the total symmetry of the hamiltonian of the system, while we so far only considered the effects of geometrical symmetry. In the classical picture, time reversal symmetry means that we can reverse the motion of all the electrons without affecting the energy structure. This is only true if all the external forces are electric forces, so that even ions with Kramers' degeneracy (Kramers ions) have their degeneracy lifted by an external magnetic field. In the QM picture it means that if we apply the timereversal operator on the Schrödinger equation, the hamiltonian of the ion is invariant provided that it contains only even powers of the momenta, that is an even number of electrons. In general, we will therefore see that RE-ions with an odd number of 4f-electrons have levels with a higher degree of degeneracy, even in a low symmetry crystal field, than the RE-ions with an even number of electrons.

3.3.5 Intensities, selection and polarization rules

Depending on the symmetry of the crystal field, the appearance of the spectrum will change; degeneracies of the J-multiplets are lifted in various degrees and new lines which for parity reasons were forbidden in the free ion, may appear. The behaviour of the hyperfine levels for each electronic J-level is however difficult to predict and is still mainly determined through a fitting of empirical values.[6]

Selection rules and polarization of emitted radiation between different J-levels can be completely predicted by the use of the previously mentioned methods. It is however not possible in this picture, to predict the behaviour of transitions between hyperfine levels belonging to different electronic levels or within the same electronic level.

A complete presentation of the polarization and selection rules between J-levels is found in [15].

3.3.6 Zeeman-splitting of hyperfine levels in $Pr^{3+} : Y_2SiO_5$

As showed in section 3.1.2, if an external magnetic field is applied, the spectrum of the ground state and excitated state hyperfine level splits up. In the material used in our experiments, $Pr^{3+} : Y_2SiO_5$, we have C_{2h} symmetry for the base unit but only axial (C_1 or D_∞) symmetry of the field at the Pr^{3+}ion sites. In table 3.1, relative oscillator strengths for the ${}^3H_4 \leftrightarrow {}^1D_2$-transition in this material have been calculated.

Since the normal oscillator strength is defined as

$$f_{ka} = \frac{2m\omega_{ka}}{3\hbar}|\mathbf{r}_{ka}|^2 \tag{3.8}$$

where

$$\mathbf{r}_{ka} = < \psi_k|\mathbf{r}|\psi_a > \tag{3.9}$$

we obtain the relative oscillator strengths by taking the square of each element in table 3.1.

When simulating a hole-burning spectrum in $Pr^{3+} : Y_2SiO_5$ we can use these oscillator strengths in order to predict the number of lines.

	-5/2	-3/2	-1/2	+1/2	+3/2	+1/2
-5/2	+0,99	+0,03	+0,09	-0,00	-0,06	+0,00
-3/2	+0,00	-0,88	-0,00	-0,19	-0,43	+0,08
-1/2	+0,07	-0,09	+0,98	-0,02	+0,18	-0,00
+1/2	-0,00	-0,18	+0,02	+0,98	-0,09	-0,07
+3/2	+0,08	+0,43	+0,19	-0,00	-0,88	-0,00
+5/2	-0,00	-0,06	-0,00	-0,09	-0,03	-0,99

Table 3.1: Overlap of nuclear states between the ground and optically excited hyperfine manifold. Columns refer to ground levels and rows to excited levels. Source [6].

Chapter 4

Experimental

4.1 Theory of experimental methods

For this attempt to measure the relative oscillator strenghts of $Pr : Y_2SiO_5$ the technique of transient spectral holeburning (TSHB) was employed. The theory of this experimental method is described in this section. For clarity, the theory of photon echoes and persistent spectral holeburning (PSHB) is also brifley outlined.

4.1.1 Photon echoes

Photon echoes is a technique of spectroscopy which was originally performed with nuclear magnetic resonance (NMR) techniques but has recently been implented in the optical regime using lasers. It is a time-domain spectroscopy, i.e. *when* the signal comes is more of interest than its precise frequency content.

Photon echoes can be generated by exposing ions to a short and intense pulse of coherent light, a so-called pump pulse. If the pulse is short, the ensemble of ions which is aimed, is coherently excited, i.e. it can be thought of as an electric dipole oscillating between the two levels; ground and excited level. If the pulse profile is the correct one, a so called $\pi/2$-pulse, the ensemble of ions will be in an equal superposition of the excited and the ground states. The wavefunctions of the ions will start to accumulate phase. As each ion has a slightly different surrounding, they also have slightly differing frequencies. Thus they will soon be out of phase with each other, in the superposed state.

If we now expose the ensemble to a second pulse of twice the area of the first one, a π-pulse; that is a pulse which would take the ensemble from the ground state completely to the excited state, the ensemble will remain in the superposed state but the accumulation of phase will be reversed. If the π-pulse comes after a delay T from the first pulse, an echo may appear after $2T$ from the first pulse.

A convenient way of understanding the action of the π-pulse on the ensemble in superposition is to adopt the view of the Bloch-sphere [16]. A π-pulse is a pulse of a duration and intensity such, that it would take the ensemble completely to the excited level, were it originally in the ground level. On the other hand, if the ensemble is already in the superposed state in between the excited and ground states, the π-pulse will take the ensemble "over the top" to

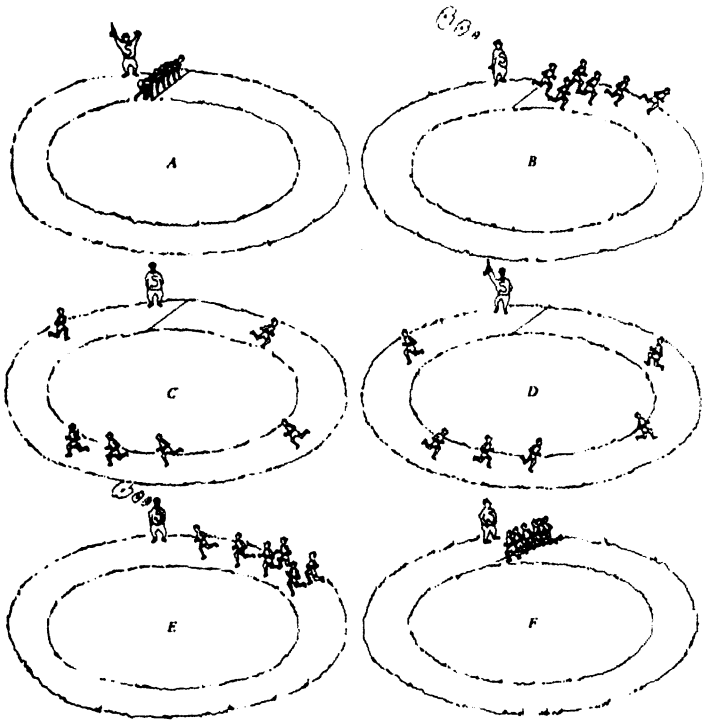

Figure 4.1: Graphical depiction of dephasing and rephasing of ions with slightly different frequency. A) During exposition to the $\pi/2$ pump pulse, all wave functions are in phase, due to the coherence of the laser pulse. B) After the $\pi/2$ pulse, the wave functions of each ion begin to cumulate phase. C) As the ions cumulate phase at different rates, they eventually get out of phase with each other. D) At the time T, the π pulse reverses the phase accumulation. F) After $2T$, all the wave functions of the ions are again in phase. A pulse of light corresponding to the initial $\pi/2$ pulse is emitted: the photon echo. Source: [16].

the excited state, then down again to the superposed level, but at a position diametrically opposite to the one it had before. This is how the accumulation of phase is reversed. Since oscillating dipoles emit radiation, a pulse of light is emitted when all the phases of all the individual dipoles (the ions) in the ensemble again are in phase, after $2T$. (See figure 4.1.)

4.1.2 Spectral holeburning

Spectral holeburning is a frequency-domain spectroscopy. It exploits the possibility lasers have to obtain very precise and narrow wavelengths to look at the relative frequency differences of close-lying sublevels within a certain transition.

Persistent spectral holeburning (PSHB)

When a strong pulse of very narrow wavelength laserlight resonant with a certain transition of some RE-ions is directed in to a REDIC-crystal, the absorptive properties of the crystal around this wavelength can be altered for a long time. In this case, a long time is in the order of seconds to minutes.

The alteration of the absorption spectrum is due to a population redistribution among the levels affected by the pump beam. In our case, the pump laser field redistributes the populations of the nuclear spin substates of the electronic ground state. The ions are first excited, then the electrons will fall back at a rate proportional to the oscillator strengths for each of the possible transitions. But since the pump field is still on, the ones falling back to the level resonant with this field will again be excited. This sublevel will eventually be "emptied", i.e. the number of electrons in this hyperfine level and its proportion to the numbers in the other two levels will have been significantly altered.

The absorption changes are monitored through a second, probe, laser field, usually a dimmed portion of the same laser beam, which is scanned in frequency around the inhomogeneously broadened resonance line. The probing field must have an intensity sufficiently low, so as not to affect the populations.

In the case of $Pr : Y_2SiO_5$, energy levels consist of three doubly degenerate nuclear spin states in both the ground and the excited levels, which produces nine different possible transitions between them. Due to the large inhomogeneous line broadening, a pump laser field can simultaneously couple to all nine possible optical transitions for nine different subsets of ions, nine different populations. See figures 4.2(a)-4.2(c).

We thus get 81 different contributions to the final holeburning spectrum, many of which are degenerate, i.e. contributions are at the same frequency, but from different ensembles of ions. Probing levels which have been emptied, i.e. where all electrons have been moved to other transitions, produce holes in the spectrum, which means a decrease in absorption at this frequency. Probing levels which have more electrons than before the burning, i.e. the levels which have recieved the electrons from the emptied levels, produce an *increase* in the absorption - these are called *antiholes.*

Transient spectral holeburning (TSHB)

In TSHB, the same burn and read-out scheme is performed as in PSHB, only the delay between the burn- and the probe-pulse is reduced to a minimum. In this way, the ions which have been excited do not have time to decay. Since we only have altered the population of one of the ground state hyperfine levels for each of the nine populations, we get a spectrum consisting of only holes and no antiholes. The number of holes are now also fewer. Of the nine possible transitions in each of the nine populations only five are affected by the pumping. There will thus be a total of 45 contributions, all of which are triply degenerate except the central one is nine-fold degenerate as before. This means 36 contributions outside the central peak, 18 on each side. The triple degeneracy finally gives us six distinct frequencies symmetrically around the center.

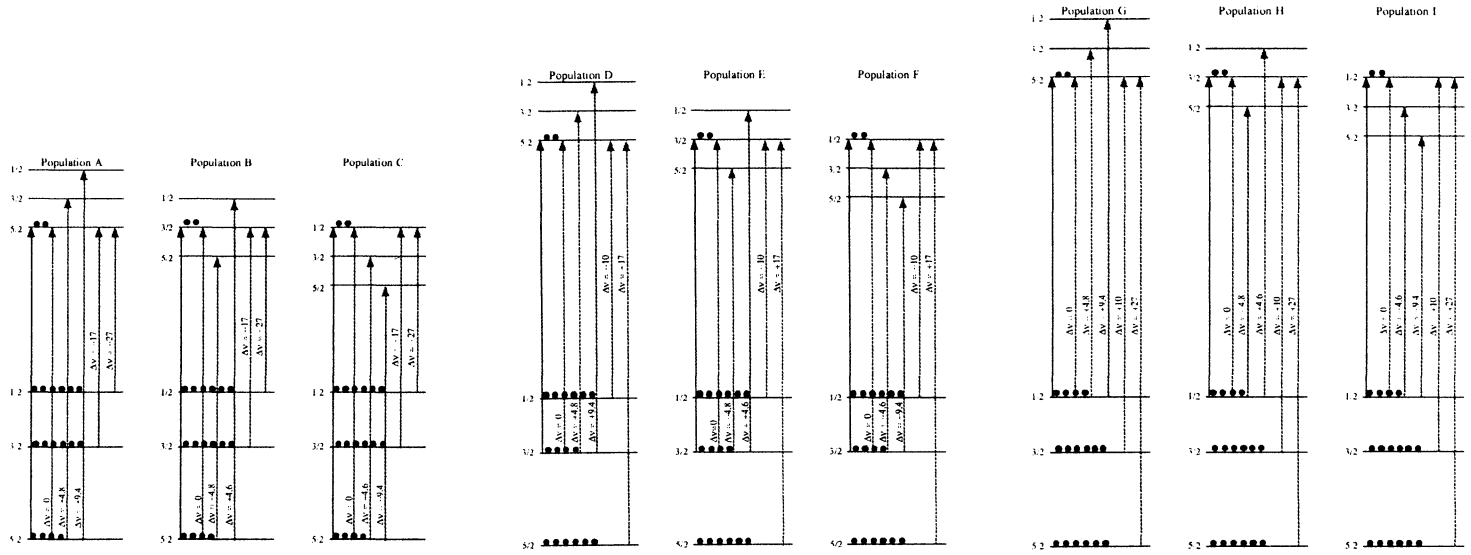

(a) Population 1-3 (b) Population 4-6 (c) Population 7-9

Figure 4.2: Diagram of the nine populations interacting with the pulses in the TSHB experiment. Burn pulse is symbolised by the leftmost, plain arrow of each population.

4.2 Equipment

4.2.1 The experimental setup

The experiments were performed using a ring dye laser pumped by an argon-ion laser. The light from the dye laser has a bandwidth of $\sim$ 1 MHz.

Pulse-shaping of the cw-light from the laser was necessary for the optical spectral hole-burning technique. A frequency sweep of the light over approx. 100 MHz was needed for the read-out of the hole. This was realised using two acousto-optic modulators (AOM) in series, driven with the same signal (see figure 4.3). The AOM's were driven by a radio-frequency (rf) signal of approximately 60 MHz. The acoustic grating inside the AOM's crystal diffracts the incoming light. The rf-signal is thereby added as sidebands to the oncoming light's frequency. We get two new frequencies after the AOM: $\nu = \nu_0 \pm \nu_{rf}$ In the zeroth order we have the frequency ν_0 and in the two first order rays, $\nu_0 + \nu_{rf}$ and $\nu_0 - \nu_{rf}$.

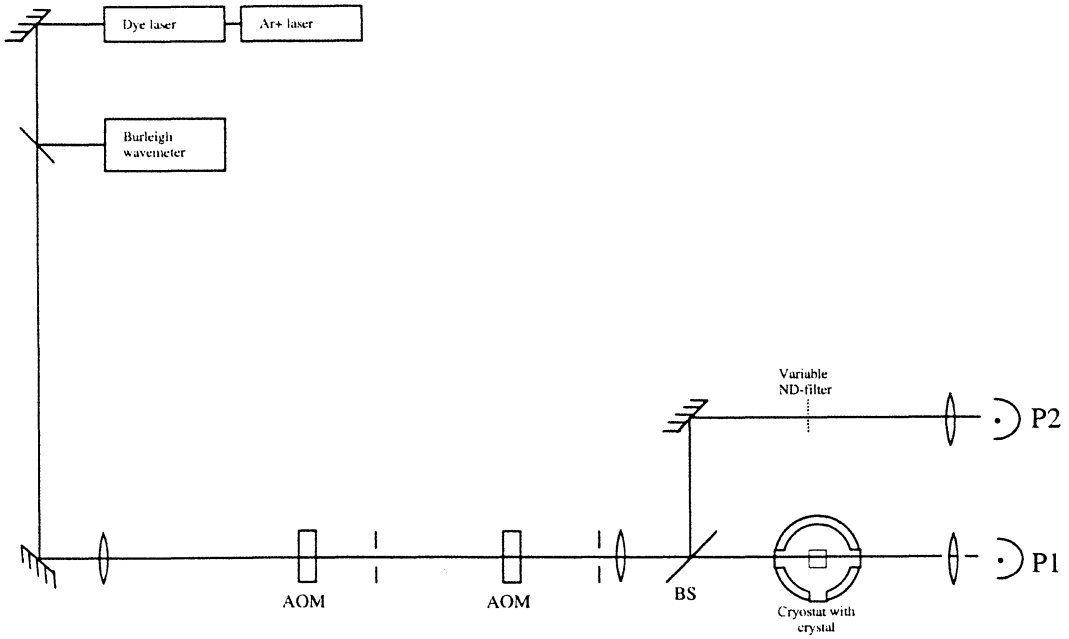

Figure 4.3: Schematic view of experimental setup

Generally, the ray which emerges on the side the acoustic wave is travelling to, has the higher frequency. By using two AOM's in series, the width of the frequency sweep of one AOM is doubled. The signal for the wavelength sweep and intensity modulation was generated by two synchronised pulse-generators. Read-out was made using two photo diodes, one for the signal from the crystal, the other registering a reference beam that was split from the pump/probe beam just before it entered the cryostat. (See fig. 4.3.) Both signals were then collected using a digital oscilloscope.

Chapter 5

Results and conclusion

5.1 The unsaturated Transient Spectral Holeburning (TSHB) spectrum

In this experience a hole is burned at a certain frequency under the ${}^3H_4 \rightarrow {}^1D_2$ inhomogeneous frequency profile.

The appearance of the unsaturated spectrum is governed by the matrix of oscillator strengths:

$$f = \begin{pmatrix} f_{55} & f_{53} & f_{51} \\ f_{35} & f_{33} & f_{31} \\ f_{15} & f_{13} & f_{11} \end{pmatrix} \tag{5.1}$$

The index *55* refers to a transition between hfs-level 5/2 in the ground state and level 5/2 in the excited state, *35* refers to a transition $|3/2\rangle_g \rightarrow |5/2\rangle_e$ etc. In this way, the rows of the matrix correspond to the three hfs-levels in the ground state and the columns to the ones in the excited state. Since transitions between levels with the same spin have a much higher probability, the oscillator strengths expressed in the diagonal elements will be much greater than the non-diagonal ones (which correspond to "forbidden" transitions).

The burn-pulse excites a certain number of ions in the nine different ion populations that are resonant with the laser frequency. The nine populations are depicted in figure 4.2.

5.1.1 Experimental data

Collection of data was made through repeated measurements of the unsaturated TSHB spectrum. Read-out was made using both integrative-averaging methods and one-shot registering of the spectrum. In figure 5.1, the measured and simulated spectra of the experiment are shown.

However, it would appear that we were not dealing with pure unsaturated TSHB, but that the measurements contained traces of saturated populations to a varying extent (see section 5.1.4 below). To alleviate these flaws in measurement we would have needed a sufficiently weak burn pulse while maintaining an acceptable S/N-ratio. In the present setup this was impossible to achieve.

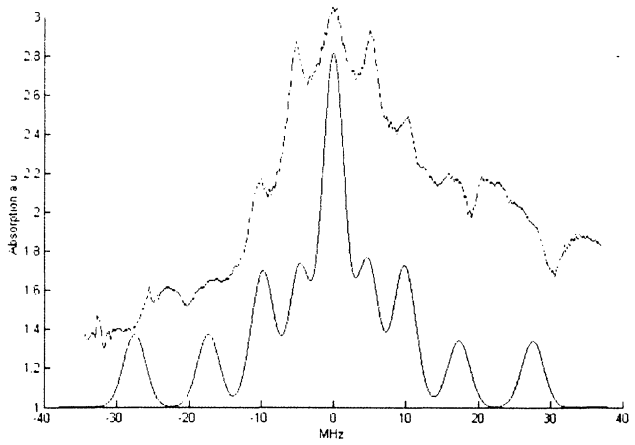

Figure 5.1: A recorded spectrum (dashed line) and a simulated one. One clearly sees the frequency correspondence between simulated and measured peeks. The assymetry of both spectra confirms our hypothesis that at least some of the measured populations were saturated. We were thus unable to perform a completely unsaturated spectrum measurement with the available setup. The misalignment of the peripheral peaks is possibly due to a non-liearity in the frequency response of the AOM's, or to their improper alignment in the setup.

5.1.2 Evaluation of experimental data

The calculation of the matrix of oscillator strengths from the intensities measured in a TSHB sequence amounts to the minimization of a non-linear equation.

The theoretical function that describes the TSHB spectrum of this transition can be constructed as follows:

Each population:*A, B, C, D, E, F, G, H, I*, contributes to five lines in the total spectrum (see figure 4.2). Each contribution from a specific population to a line at a certain frequency is thus proportional to the product of two oscillator strengths: one for the transition resonant with the burn pulse and one for the transition at which the read-out occurs for this line. The function that determines the spectrum must therefore contain $9 * 5 = 45$ pairwise products of the oscillator strengths of the matrix f above. However, in the unsaturated TSHB, 36 of these pairs are doubly degenerate due to the commutability of the products $f_{i,j}f_{k,l}$. In effect, each product appears once on each side of, and at equal distances to, the central peak at $\nu_0 = 0MHz$. In this way, the term $f_{55}f_{35}$ will give a contribution to the peak at $-17MHz$ while the commuted term $f_{35}f_{55}$ will add to the $+17MHz$ peak. All product pairs with identical elements, e.g. $f_{33}f_{33}$ will only appear once for each population. This is the contribution to the central peak (burn and read-out at the same frequency).

The terms of the generating function of the TSHB spectrum are listed below. In this enumeration the following definitions have been made:

The function $L(\nu, \nu_0)$ is a function that generates a lineshape around a central frequency, ν_0. It's a normalized and smooth intensity function for a line centred at an arbitrary frequency position, that is:

$$
\begin{aligned}
L(\nu) &: \Re \to \Re;\ D(L) \in \Re \text{ and } V(L) \in (0,1] \\
\|L\|_\infty &= 1 \\
\frac{dL}{d\nu}L &\neq \pm\infty
\end{aligned}
$$

The function L is chosen to be a lorentzian:

$$L(\nu, \nu_0) = \frac{1}{1 + (\nu - \nu_0)^2}$$

as this is the lineshape atomic theory predicts. The dimension of the argument of L is MHz. Thus we have a lorentzian with a full-width, half-maximum (FWHM) value of 2 MHz. To closer fit the experimental read-outs, this linewidth is modified in the numerical treatment of data.

We introduce m as a constant with an arbitrary value between 0 and 1. It corresponds to the average absorption level over the frequency range in question. The functions describing the contributions to the total spectrum from each of the nine populations then are (the index letter of the individual generating function refers to the population):

$$
\begin{aligned}
S_A(f) &= m \cdot f_{55}[2 \cdot f_{55}L(0) + f_{53}L(+4.8) + \\
&\quad f_{51}L(+9.4) + f_{35}L(-17.3) + f_{15}L(-27.5)]
\end{aligned}
$$

$$
\begin{aligned}
S_B(f) &= m \cdot f_{53}[f_{55}L(-4.8) + 2 \cdot f_{53}L(0) + \\
&\quad f_{51}L(+4.6) + f_{33}L(-17.3) + f_{13}L(-27.5)]
\end{aligned}
$$

$$
\begin{aligned}
S_C(f) &= m \cdot f_{51}[f_{55}L(-9.4) + f_{53}L(-4.6) + \\
&\quad 2 \cdot f_{51}L(0) + f_{31}L(-17.3) + f_{11}L(-27.5)]
\end{aligned}
$$

$$
\begin{aligned}
S_D(f) &= m \cdot f_{35}[f_{55}L(+17.3) + 2 \cdot f_{35}L(0) + \\
&\quad f_{33}L(+4.8) + f_{31}L(+9.4) + f_{15}L(-10.2)]
\end{aligned}
$$

$$
\begin{aligned}
S_E(f) &= m \cdot f_{33}[f_{53}L(+17.3) + f_{35}L(-4.8) + \\
&\quad 2 \cdot f_{33}L(0) + f_{31}L(+4.6) + f_{13}L(-10.2)]
\end{aligned}
$$

$$
\begin{aligned}
S_F(f) &= m \cdot f_{31}[f_{51}L(+17.3) + f_{35}L(-9.4) + \\
&\quad f_{33}L(-4.6) + 2 \cdot f_{31}L(0) + f_{11}L(-10.2)]
\end{aligned}
$$

$$
\begin{aligned}
S_G(f) &= m \cdot f_{15}[f_{55}L(+27.5) + f_{35}L(+10.2) + \\
&\quad 2 \cdot f_{15}L(\nu = 0) + f_{13}L(+4.8) + f_{11}L(+9.4)]
\end{aligned}
$$

$$
\begin{aligned}
S_H(f) &= m \cdot f_{13}[f_{53}L(+27.5) + f_{33}L(+10.2) + \\
&\quad f_{15}L(-4.8) + 2 \cdot f_{13}L(\nu = 0) + f_{11}L(+4.6)]
\end{aligned}
$$

$$\begin{aligned} S_I(f) &= m \cdot f_{11}[f_{51}L(+27.5) + f_{31}L(+10.2) + \\ &\quad f_{15}L(-9.4) + f_{13}L(-4.6) + 2 \cdot f_{11}L(\nu_0 = 0)] \end{aligned}$$

The total spectrum is the sum of these nine contributions.

$$S(f) = S_A(f) + S_B(f) + ... + S_I(f) \tag{5.2}$$

For the calculation of the empirical oscillator strengths this function needs to be fitted to the experimental spectra. In order to facilitate the numerical fitting of a curve to the measured spectrum, some simplification of the generating function is needed.

Let us therefore look at the contributions to the spectrum at each of the thirteen different frequency locations: 0MHz, ±4.6MHz, ±4.8MHz, ±9.4MHz, ±10.2MHz, ±17.3MHz, ±27.5MHz. If the contributions to each of the lines are considered linearly independent from each other, we get the following system of equations:

$$\begin{aligned}
F(+27.5) &= m[f_{15}f_{55} + f_{13}f_{53} + f_{11}f_{15}]L(+27.5) \\
F(-27.5) &= m[f_{55}f_{15} + f_{53}f_{13} + f_{15}f_{11}]L(-27.5) \\
F(+17.3) &= m[f_{35}f_{55} + f_{33}f_{53} + f_{31}f_{51}]L(+17.3) \qquad (5.3) \\
F(-17.3) &= m[f_{55}f_{35} + f_{53}f_{33} + f_{51}f_{31}]L(-17.3) \qquad (5.4) \\
F(+10.2) &= m[f_{15}f_{35} + f_{13}f_{33} + f_{11}f_{31}]L(+10.2) \\
F(-10.2) &= m[f_{35}f_{15} + f_{33}f_{13} + f_{31}f_{11}]L(-10.2) \\
F(+9.4) &= m[f_{55}f_{51} + f_{35}f_{31} + f_{15}f_{11}]L(+9.4) \\
F(-9.4) &= m[f_{51}f_{55} + f_{31}f_{35} + f_{11}f_{15}]L(-9.4) \\
F(+4.8) &= m[f_{55}f_{53} + f_{35}f_{33} + f_{15}f_{13}]L(+4.8) \\
F(-4.8) &= m[f_{53}f_{55} + f_{33}f_{35} + f_{13}f_{15}]L(-4.8) \\
F(+4.6) &= m[f_{53}f_{51} + f_{33}f_{31} + f_{15}f_{11}]L(+4.6) \\
F(-4.6) &= m[f_{51}f_{53} + f_{31}f_{33} + f_{11}f_{15}]L(-4.6) \\
F(0) &= m[f_{55}^2 + f_{53}^2 + f_{51}^2 + \\
&\quad f_{35}^2 + f_{33}^2 + f_{31}^2 + \\
&\quad f_{15}^2 + f_{13}^2 + f_{11}^2]L(0)
\end{aligned}$$

Symmetry of the spectrum

From this model, we can see that the unsaturated TSHB spectra must always be symmetric. In effect, if we look at a pair of complementary frequencies, say +17.3 MHz and -17.3 MHz (equations 5.3 - 5.4), we see that the product of oscillator strengths which are the terms in F(-17.3) are the same as those in F(+17.3), only with commuted factors.

5.1.3 Numerical treatment of data

From the experimental data, we conclude that the probing laser has a band width of approximately 2 MHz, at best. Therefore the double peaks at ±4.6

and ± 4.8 MHz and the ones at $\pm 9.4, \pm 10$ MHz are not resolved. However, the nine resulting peaks are sufficiently far from each other to be clearly resolved. It is therefore a fair approximation to consider the equations governing the intensity contribution at each of these nine frequencies as linearly independant. The system of equations then becomes

$$\left\{\begin{array}{rcl} F(+27.5) & = & m[f_{15}f_{55} + f_{13}f_{53} + f_{11}f_{15}]L(+27.5) \\ F(-27.5) & = & m[f_{55}f_{15} + f_{53}f_{13} + f_{15}f_{11}]L(-27.5) \\ F(+17.3) & = & m[f_{35}f_{55} + f_{33}f_{53} + f_{31}f_{51}]L(+17.3) \\ F(-17.3) & = & m[f_{55}f_{35} + f_{53}f_{33} + f_{51}f_{31}]L(-17.3) \\ F(+10) & = & m[f_{15}f_{35} + f_{13}f_{33} + f_{11}f_{31} + \\ & & f_{55}f_{51} + f_{35}f_{31} + f_{15}f_{11}]L(+10) \\ F(-10) & = & m[f_{35}f_{15} + f_{33}f_{13} + f_{31}f_{11} + \\ & & f_{51}f_{55} + f_{31}f_{35} + f_{11}f_{15}]L(-10) \\ F(+5) & = & m[f_{55}f_{53} + f_{35}f_{33} + f_{15}f_{13} + \\ & & f_{53}f_{51} + f_{33}f_{31} + f_{15}f_{11}]L(+5) \\ F(-5) & = & m[f_{53}f_{55} + f_{33}f_{35} + f_{13}f_{15} + \\ & & f_{51}f_{53} + f_{31}f_{33} + f_{11}f_{15}]L(-5) \\ F(0) & = & m[f_{55}^2 + f_{53}^2 + f_{51}^2 + \\ & & f_{35}^2 + f_{33}^2 + f_{31}^2 + \\ & & f_{15}^2 + f_{13}^2 + f_{11}^2]L(0) \end{array}\right. \tag{5.5}$$

To deduce the matrix f of oscillator strengths from the above system is a problem of non-linear optimization. We have nine populations which each generate five lines, that is five pairs of f_{ij}'s, for a total of forty-five pairs. As we saw, thirty-six of these are pair-wise identical. All product-pairs with both factors identical, e.g. $f_{53}f_{53}$, appear only once, at the central (zero) peak. This reduces the number of different products $f_{ij}f_{kl}$ to twenty-seven.

Because of the quadratic nature of the $f_{ij}f_{kl}$-terms, the generating function 5.2 cannot be factorized. This complicates matters with respect to optimization, since the function behaves as if it has twenty-seven linearly independent (although not completely) parameters. The matrix of relative oscillator strengths, f, has normalized row- and column sums, which give us six constraints that can help reduce the system.

$$\left\{\begin{array}{rcl} f_{55} + f_{53} + f_{51} & = & 1 \\ f_{35} + f_{33} + f_{31} & = & 1 \\ f_{15} + f_{13} + f_{11} & = & 1 \\ f_{55} + f_{35} + f_{15} & = & 1 \\ f_{53} + f_{33} + f_{13} & = & 1 \\ f_{51} + f_{31} + f_{11} & = & 1 \end{array}\right. \tag{5.6}$$

From these constraints, one can chose four variables as parameters, to generate the entire matrix. For example, if we chose the four elements of the lower right-hand corner of f; f_{33}, f_{31}, f_{13} and f_{11}, as parameters we get:

$$\left\{\begin{array}{rcl} f_{55} & = & f_{33} + f_{31} + f_{13} + f_{11} - 1 \\ f_{53} & = & 1 - f_{33} - f_{13} \\ f_{51} & = & 1 - f_{31} - f_{11} \\ f_{35} & = & 1 - f_{33} - f_{31} \\ f_{15} & = & 1 - f_{13} - f_{11} \end{array}\right. \tag{5.7}$$

In order to try to deduce the oscillator strengths from the recorded spectra, a theoretical spectrum was first created, from a choice of four parameters that fulfill the constraints in 5.7. A scalar function was created whose out-data was the sum of the squared differences between the theoretical and the empirical spectra vectors. A non-linear minimization with constraints was then performed on this function, using the simplex method implemented in Matlab's 'fminsearch' routine. As this is a poorly conditioned problem, it was found that the outcome of the iteration proces was highly dependant on the choice of initial guess, the "seed". This means the objective function contains a large number of local minima inside the domain.

5.1.4 Saturation

One surprising aspect of the experiment was the frequent recording of asymmetric spectra. The possible explanations of this asymmetry are;

1. Ground-state levels are unequally populated initially.
2. Saturation of one or more of the pumped transitions.

Due to the large value of kT ($2.8cm^{-1}$), and the fact that the pumping laser was continuously swept over the inhomogeneous frequency band, the first suggestion seems much more unlikely than the second. The comparison of spectra made with pump pulses of different duration leads to believe the second hypothesis to be correct.

If we trace each and every term in the generating function 5.2 back to its population, we can, at least qualitatively, explain this asymmetric appearance. Since the conditions for the mathematical generating function no longer apply, the model breaks down. If equation 5.5 is marked up with an extra index pertaining to the population, we get:

$$
\begin{aligned}
F(+27.5) &= m[f_{15}^G f_{55}^G + f_{13}^H f_{53}^H + f_{11}^I f_{15}^I]L(+27.5) \\
F(-27.5) &= m[f_{55}^A f_{15}^A + f_{53}^B f_{13}^B + f_{51}^C f_{11}^C]L(-27.5) \\
F(+17.3) &= m[f_{35}^D f_{55}^D + f_{33}^E f_{53}^E + f_{31}^F f_{51}^F]L(+17.3) \\
F(-17.3) &= m[f_{55}^A f_{35}^A + f_{53}^B f_{33}^B + f_{51}^C f_{31}^C]L(-17.3) \\
F(+10) &= m[f_{15}^G f_{35}^G + f_{13}^H f_{33}^H + f_{11}^I f_{31}^I + \\
&\quad f_{55}^A f_{51}^A + f_{35}^D f_{31}^D + f_{15}^G f_{11}^G]L(+10) \qquad (5.8) \\
F(-10) &= m[f_{35}^D f_{15}^D + f_{33}^E f_{13}^E + f_{31}^F f_{11}^F + \\
&\quad f_{51}^C f_{55}^C + f_{31}^F f_{35}^F + f_{11}^I f_{15}^I]L(-10) \qquad (5.9) \\
F(+5) &= m[f_{55}^A f_{53}^A + f_{35}^D f_{33}^D + f_{15}^G f_{13}^G + \\
&\quad f_{53}^B f_{51}^B + f_{33}^E f_{31}^E + f_{13}^H f_{11}^H]L(+5) \\
F(-5) &= m[f_{53}^B f_{55}^B + f_{33}^E f_{35}^E + f_{13}^H f_{15}^H + \\
&\quad f_{51}^C f_{53}^C + f_{31}^F f_{33}^F + f_{11}^I f_{13}^I]L(-5) \\
F(0) &= m[(f_{55}^A)^2 + (f_{53}^B)^2 + (f_{51}^C)^2 + \\
&\quad (f_{35}^D)^2 + (f_{33}^E)^2 + (f_{31}^F)^2 + \\
&\quad (f_{15}^G)^2 + (f_{13}^H)^2 + (f_{11}^I)^2]L(0)
\end{aligned}
$$

Saturation in a two-level system occurs, by definition, when 1/4 of the total population of absorbing atoms is in the excited state. The rate of absorption is then significantly decreasing. The result in our case is that the other eight populations, which have a different resonant transition will recieve proportionally more light. As they are submitted to a stronger pumping field, this will excite more electrons. At read-out, the contributions from these populations will no longer be proportional to their true relative oscillator strength. A contribution from a weak transition will look stronger, as it has been subject to a stronger field. Its corresponding oscillator strength will then appear greater than it is. Saturation also poses a problem to the row- and column-normalization constraint imposed upon the f-matrix. Although these constraints are by definition true for the isolated ion, it is no longer meaningful for the population, since the field no longer can be considered to be constant.

As an effect of the failure of the normalization constraint for the ensemble, the product pairs $f_{ij}f_{kl}$ will no longer commute.

$$f_{ij}^N f_{kl}^N \neq f_{kl}^M f_{ij}^M, \ M,N = A,B,...,I \tag{5.10}$$

This is directly caused by the non-uniformity of the field. For example, if the population with index I is saturating, $f_{11}f_{15}$ will appear to have a certain, rather large, value. For population G, which contains the element $f_{15}f_{11}$, this product may have a totally different value, since the $1/2 \rightarrow 1/2$ transition for this population is not resonant with the pump pulse, and since the pumped $1/2 \rightarrow 5/2$ transition sees more light than population I (see figure 4.2(c)). In brief, the f's no longer commute, since they become population dependant, e.g.:

$$f_{11}^I \neq f_{11}^C$$

The $1/2 \rightarrow 1/2$, $3/2 \rightarrow 3/2$ and $5/2 \rightarrow 5/2$-transitions are the most likely to saturate, since the diagonal elements of the matrix of oscillator strengths (equation 5.1) are much greater than the other elements. Let's look at the 10 MHz peaks, equations 5.8 and 5.9, since this seems to be the ones most responsible for the asymmetry. For example, imagine the $1/2 \rightarrow 1/2$-transition is saturating. This is population I. More light will then go to the other populations. At +10MHz populations A, D, G, G, H and I are contributing. At -10 MHz populations C, D, E, F, F and I. If the contributions from population I to both peaks is estimated to be equal, it is the sum of the other contributions that determine the asymmetry. Because of 5.10, all the terms in these two sums, equations 5.8 and 5.9 of the system 5.5 can have different values, and the assymmetry is possible.

Simulations of unsaturated spectra were made using the methods described above in section 5.1.3 by introducing scalar "saturation factors", different for each population. An example of such a simulation is seen in figure 5.1.

5.1.5 Outlook; an other way of performing the measurement.

A better measurement of the oscillator strengths of $Pr3+$ in YSO, would be to first empty two of the three ground state hfs-levels. Before doing so, a "well" has to be burned with a width of about 10MHz. The ions that will be measured

are then placed in the center of the well by burning another hole at a distance of 27 MHz. It is the ions in the sidehole of this hole, that will be measured.

The ions at the center of the well consist of three populations. The peak that appears in the middle of the well is the -27 MHz peak which comes from populations resonant at the $|5/2\rangle_g \rightarrow |5/2\rangle_e$, the $|5/2\rangle_g \rightarrow |3/2\rangle_e$ and the $|5/2\rangle_g \rightarrow |1/2\rangle_e$ transitions. With these ions we would always be exciting from only one ground state hfs-level, but we still have three different upper levels, due to the three populations.

The generating function that describes the spectrum will thus only have terms from populations A, B, C in equation system 5.5:

$$\begin{aligned}
F(+27.5) &= m[0]L(+27.5) \\
F(-27.5) &= m[f_{55}^A f_{15}^A + f_{53}^B f_{13}^B + f_{51}^C f_{11}^C]L(-27.5) \\
F(+17.3) &= m[0]L(+17.3) \\
F(-17.3) &= m[f_{55}^A f_{35}^A + f_{53}^B f_{33}^B + f_{51}^C f_{31}^C]L(-17.3) \\
F(+10) &= m[f_{55}^A f_{51}^A]L(+10) && (5.11) \\
F(-10) &= m[f_{51}^C f_{55}^C]L(-10) && (5.12) \\
F(+5) &= m[f_{55}^A f_{53}^A + f_{53}^B f_{51}^B]L(+5) && (5.13) \\
F(-5) &= m[f_{53}^B f_{55}^B + f_{51}^C f_{53}^C]L(-5) && (5.14) \\
F(0) &= m[(f_{55}^A)^2 + (f_{53}^B)^2 + (f_{51}^C)^2 +]L(0) && (5.15)
\end{aligned}$$

From equations 5.11, 5.12 we see that the peaks at 10 MHz would give us directly the product of the f-elements $f_{55}^A f_{51}^A$ and $f_{51}^C f_{55}^C$. Unfortunately, these peaks will be overlapping the sideholes at -17.3 MHz belonging to the preparation hole burned at -27MHz, and will probably not be useful for measurement. The only peaks which appear inside the well will be the ± 5 MHz peaks. These, together with the central peaks will give us information of the products in equations 5.13 - 5.15. The objective function to minimize would then be the the difference between the vector of measured values and the sum of the terms in 5.13 - 5.15.

$$\begin{aligned}
S_{A,B,C}(f) &= m \cdot f_{55}[2 \cdot f_{55}L(0) + f_{53}L(+4.8)] \\
&\quad + m \cdot f_{53}[f_{55}L(-4.8) + 2 \cdot f_{53}L(0) \\
&\quad + f_{51}L(+4.6)] + m \cdot f_{51}[f_{53}L(-4.6) \\
&\quad + 2 \cdot f_{51}L(0)]
\end{aligned}$$

5.1.6 Conclusion

It is thus not possible to calculate the definite values of the f-matrix using the simplex method. It might, however, be possible to find an over all minimum using some other algorithm, for instance a simulated annealing method. Investigating this and other numerical recipes falls outside the time-frame of this project and is thus left for other workers.

Acknowledgments

I would like to thank Stefan Kröll, the members of the photon-echo group and my fellow diploma-workers for their practical help, exchange of ideas, cheerful chats and readiness to discuss the problems encountered.

I would also especially like to thank my father for his moral support during the elaboration of this work.

Bibliography

[1] Einstein, A., Podolsky, B. & Rosen, N. *Can Quantum-Mechanical Description of Physical Reality Be Considered Complete?* Phys. Rev. **47**, 777 (1935).

[2] Bouwmeester, D., Ekert, A. & Zeilinger, A., *The Physics of Quantum Information* Springer-Verlag, Berlin, (2000).

[3] Julsgaard, B., Kozhekin, A. & Polzik, E. *Experimental long-lived entanglement of two macroscopic objects* Nature **413**, 27 Sept. 2001, pp. 400-403.

[4] Silverberg, L., Gislen, L., Bengtsson, H.-U. *Inledande kvantmekanik*, kompendium, Institutionen för teoretisk fysik, Lunds Universitet.

[5] Garcia, D., Faucher, M. *Handbook on the Physics and Chemistry of the Rare Earths.*

[6] Longdell, J. J., Sellars, M. J., Manson, N. B. *Hyperfine interaction in ground and excited states of praseodymium-doped yttrium orthosilicate* Phys. Rev. B **66**, 035101 (2002).

[7] Abragam, A. and Bleaney, B. *Electron Paramagnetic resonance of transition ions* Clarendon Press, Oxford, (1970).

[8] Klintenberg, M., Edvardsson, S. and Thomas, J., O. *Calculation of energy levels and polarized oscillator strengths for* $Nd^{3+} : YAG$. Phys. Rev. B **55**, 10369 (1997)

[9] Åberg, D. and Edvardsson, S. *Direct calculation of optical absorption amplitudes for trivalent rare-earth ions in* $LiYF_4$. Phys. Rev. B **65**, 045111 (2002)

[10] Edvardsson, S., Klintenberg, M. and Thomas, J., O. *Use of polarized optical absorption to obtain structural information for* $Na^+/Nd^{3+}\beta$*-alumina.* Phys. Rev. B **54**, 17476 (1996).

[11] Duan, Lu-Ming, Cirac, J. I. Zoller, P. and Polzik, E. S. *Quantum Communication between Atomic Ensembles Using Coherent Light* Phys. Rev. Lett. **85**, 5643 (2000).

[12] Julsgaard, B., Kozhekin, A. and Polzik, E. S. *Experimental long-lived entanglement of two macroscopic objects* Nature **413**, 400 (2001).

[13] Lukin, M. D. and Hemmer, P. R. *Quantum Entanglement via Optical Control of Atom-Atom Interactions* Phys. Rev. Lett. **84**, 2818 (2000).

[14] Hecht, E. and Zajac, A. *Optics* Addison-Wesley Publishing Company Inc. (1974).

[15] Dieke, G. H. *Spectra and Energy Levels of Rare Earth Ions in Crystals* John Wiley & Sons, New York (1968).

[16] Allen, L. & Eberly J. H. *Optical resonance and two-level atoms* John Wiley & Sons, New York (1975).

[17] Bell, J. S. *Speakable and unspeakable in quantum mechanics* Cambridge University Press (1987).

[18] Bransden, B. H. & Joachain, C. J. *Introduction to Quantum Mechanics* Longman Scientific & Technical (1989).

[19] Ohlsson, N., Mohan, R. K. and Kröll, S. *Quantum computer hardware based on rare-earth-ion-doped inorganic crystals*, Optics Commun. **201**, 71 (2002)

[20] Barenco, A., Ekert, A., Sanprera, A. & Machiavello, C. *Un saut d'echelle pour les calculateurs* La Recherche, Nov 1996.

[21] Svanberg, S. *Atomic and Molecular Spectroscopy - basic aspects and practical applications* Springer-Verlag (2001).

[22] Graf, F. R. *Investigations of spectral dynamics in rare earth ion doped crystals using high resolution laser techniques* Diss. ETH No 12623, Zürich, (1998)

[23] Wybourne, B. G. *Spectroscopic Properties of Rare Earths* Interscience, New York (1965).

[24] E. Biémont, P. Quinet, Z. Dai, Jiang Zhankui, H. Xu, S. Svanberg, *Lifetime measurements and calculations in singly ionized ytterbium*, J. Phys. B: At. Mol. Opt. Phys. **35**, 4743 (2002).

[25] Biémont, E. and Quinet, P. *Recent advances in study of lanthanide atoms and ions*, Phys. Scr. T105, 38 (2003).

Index